Wave Digital Models of Piezoelectric Transducers for Audio Applications

Riccardo Giampiccolo, *Graduate Student Member, IEEE*, Alberto Bernardini, *Member, IEEE*, Augusto Sarti, *Senior Member, IEEE*

***Abstract*— The number of consumer electronics devices integrating piezoelectric (PE) transducers as flat-panel loudspeakers has recently experienced a steep increase. Being very thin, in fact, piezoelectric transducers well cope with the miniaturization process that characterizes the market. However, at the same time, their reduced dimensions cause the sound pressure level to be poor at low frequency, impairing the overall acoustic response. In this paper, we derive novel efficient discrete-time models of PE transducers in the Wave Digital (WD) domain such that they can be integrated in the future into signal processing algorithms for audio output enhancement. WD Filters are, in fact, making headway among audio digital signal processing techniques based on circuit equivalent models thanks to their efficiency, robustness, and accuracy. Starting from circuital representations of the piezo constitutive equations, we derive both lumped and distributed models. In particular, we show how it is possible to implement the frequency-dependent elements characterizing Mason's model in the WD domain, contrary to what can be done using mainstream Spice-like simulators. Such WD implementations come in handy for the simulation and fast prototyping of PE systems, paving the way toward the design of model-based digital signal processing algorithms for enhancing the transducer acoustic performance.**

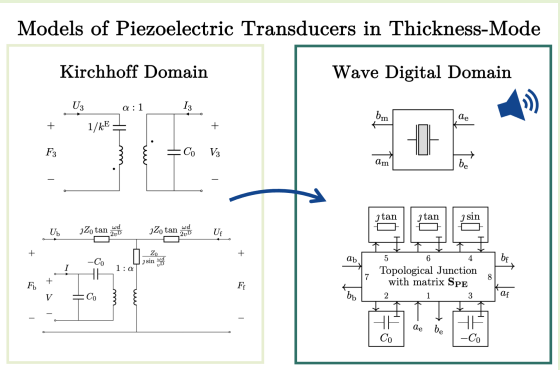

***Index Terms*— Wave Digital Filters, piezoelectric transducers, audio applications, consumer electronics.**

I. Introduction

OVER the past few years, an ever-increasing interest has been put into consumer electronics applications involving piezoelectric (PE) transducers. Such devices are paving the way towards the design of more compact and lightweight products, without sacrificing accuracy, sensitivity, and bandwidth [1]. For instance, PE transducers have gained a foothold as biomedical [2], haptic [3], and pressure/fingerprint [4], [5] sensors, as well as energy harvesting devices [6]. Among the different areas, however, PE transducers are showing to be particularly appealing for audio applications [7]. Their thin profile, in fact, makes them suitable to be integrated as flat-panel loudspeakers in televisions [8], [9], headphones [10], and, more generally, in portable devices [11], which are subjected to a continuous miniaturization process. Moreover, thanks to their capacitive nature, piezos are more power efficient than standard dynamic loudspeakers [8] and, contrary to the latter, their nodal distribution and radiance pattern is modified according to the way they are fastened (i.e., to their rigidity), being thus intrinsically able to accommodate beamforming techniques [7]. In the future, they could completely replace microspeakers, making smartphones, tablets, and laptops more robust, durable, and waterproof. However, the market trend, that encourages the miniaturization of portable devices, jeopardizes at the same time the response of piezoelectric speakers. In fact, the smaller the radiating surface, the lower the Sound Pressure Level (SPL) at low frequencies, and thus the harder to obtain full-audio-range transducers. In order to tackle this problem, several design attempts are present in the literature [12], [13]. Such approaches, however, might be subjected to a higher manufacturing cost and product size, justifying research effort towards digital signal processing methodologies able to enhance the acoustic performance of PE devices. To this aim, psychoacoustic techniques are sometimes employed to create the illusion of a tone below the cut-off frequency of the piezo exploiting the "missing fundamental" phenomenon [14], [15]; other times, a simple dynamic range compressor is employed to flatten the SPL [15]. In this context, efficient, stable, and algorithm-oriented digital realizations of PE transducer models are desirable since they can be integrated into digital signal processing techniques to obtain better performance by leveraging the physics of the device.

In this manuscript, we derive novel discrete-time models of PE transducers by exploiting Wave Digital Filter (WDF) principles [16]. WDFs have gained popularity in the field of digital audio processing, especially in the context of Virtual Analog

This work was funded and supported by INVENTVM Semiconductor s.r.l., Via Alessandro Brambilla, 60, 27100, Pavia (PV), Italy.

R. Giampiccolo, A. Bernardini, and A. Sarti are with the Dipartimento di Elettronica, Informazione e Bioingegneria (DEIB), Politecnico di Milano, Piazza L. Da Vinci 32, 20133, Milano, Italy. Corresponding author: Riccardo Giampiccolo (email: riccardo.giampiccolo@polimi.it).

modeling [17]. WDFs [16] were introduced by A. Fettweis in the late '70s for designing stable and passive digital filters starting from their analog counterparts. The design of a WDF implies that each pair of Kirchhoff port variables (i.e., port voltage and port current) in the reference circuit is substituted with a linear combination of incident and reflected waves with one extra free parameter per port called *port resistance*. One-port and multi-port circuit elements are represented by means of one-port and multi-port Wave Digital (WD) blocks characterized by input-output scattering relations [18]. The interconnections among elements, instead, are realized by means of N-port WD topological junctions, called *adaptors* [19]. Dynamic elements (e.g., inductors and capacitors) are typically realized using stable discretization methods, such as the trapezoidal rule or the Backward Euler method. Implicit relations between incident and reflected waves (called *delay-free-loops* in the WDF literature) can be eliminated by properly setting the free parameter at each port, i.e., by performing the so called *adaptation* process [19]. Hence, differently to what happens dealing with Spice-like software, most linear circuits [18] and certain circuits containing at most one nonlinear element [20], [21] can be modeled as fully explicit WD structures based on stable discretization methods. WD realizations of other circuits, including networks with multiple nonlinearities, instead, also require to use iterative solvers [22]–[27]. However, even in these cases, WD techniques offer interesting advantages over traditional simulation techniques working in the Kirchhoff domain, especially thanks to the ability of separately handling topology and element descriptions [28] and the possibility to conveniently set the free parameters (port resistances) in order to speed-up convergence and increase the robustness of the iterative methods [22], [23], [29].

PE transducers are usually described by a system of tensorial equations [30], which may reduce to a scalar system of equations if the hypothesis of thickness-mode (i.e., thickness much smaller than the other two dimensions) is fulfilled. Due to the thin profile required by recent audio applications, the thickness-mode hypothesis is assumed to be always valid. Several linear models of thickness-mode piezoelectric transducers are present in the literature: some of them are lumped models derived exploiting the hypothesis of quasi-static regime (i.e., stress and strain constant along the piezoelectric plate) [12], [31], others are described as distributed models [32], [33]. Among distributed models, some of them are derived as equivalent circuits [12], [32], others expressing physical variables in the discrete-time domain [34], [35], and still others as block diagrams [36]. The various kinds of models mainly differ one from the other according to the region of the spectrum in which the piezo is operated. Lumped models can be derived only if the frequencies into play are much lower than the first resonant mode frequency of the piezo itself. If this does not hold true, the hypothesis of quasi-static regime is not valid and a distributed model has to be considered in order to take into account the propagation of acoustic waves inside the PE medium.

In this paper we consider both lumped and distributed models. The realization of such models in the WD domain

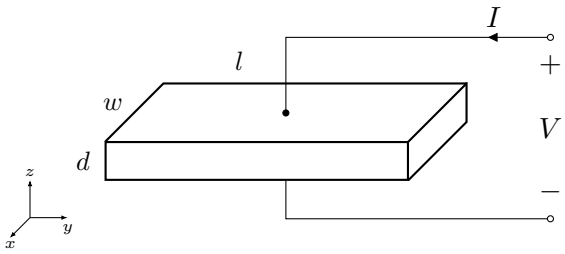

Fig. 1. Piezoelectric plate poled and excited along the z-axis. Thickness-mode operation is valid only if $\boldsymbol{d} \ll \boldsymbol{l} \wedge \boldsymbol{d} \ll \boldsymbol{w}$ holds true.

paves the way, on the one hand, to exploit efficient and robust WD methods for the simulation of PE systems [24], [37], and, on the other hand, to integrate the models into real-time digital audio algorithms. Examples of applications would be the equalization or the linearization of audio systems via circuital inversion [38]. In this regard, it has been shown in [39], [40] that WDFs can be fruitfully employed for implementing digital inverse models of loudspeaker equivalent circuits, which, in turn, can be used to design algorithms of loudspeaker equalization, linearization, and virtualization. Besides simulation and fast prototyping purposes, we therefore aim at deriving WD implementations of direct and inverse PE transducers suitable to be integrated in algorithms similar to the ones presented in [39], [40].

The manuscript is organized as follows. Section II deals with theoretical background on piezoelectric transducers in thickness-mode. Section III presents a background on some useful notions of WDF theory. In Section IV, lumped models of PE transducers are described under the hypothesis of quasi-static regime; WD realizations of such models are then derived proposing different solutions according to the degree of accuracy required by the application. Section V, instead, presents a possible WD implementation of Mason's distributed model [32] and shows that it is possible to realize its frequency-dependent components in the discrete-time domain still using a block-based approach, contrary to what can be done in mainstream Spice-like circuit simulators [41]. Numerical examples are then provided in Section VI, whereas Section VII concludes this paper.

II. Theoretical Background on Thickness-mode Piezoelectric Transducers

Piezoelectricity is a property of non-centrosymmetric crystals, i.e., of those crystals with no inversion symmetry, that results from the interaction between mechanical and electrical states [32]. In this work, we consider such an interaction to be linear. The piezoelectric effect is said to be *direct* if given a mechanical strain an electrical field is generated, or *converse* if given an electrical field a mechanical strain is generated. Many materials show a relevant piezoelectric effect only after being subjected to *poling*, whose aim is to orient the electric dipoles along a common direction such that the changes in the crystalline structure generate a macroscopic effect. By convention, the axis on which the poling is performed is marked with index number 3, and, in our discussion, it will

always be the z-axis. The electroacoustic transduction can be achieved by exploiting the converse piezoelectric effect. Leaving out, for the sake of clarity, the time dependence, the mechanical stress T and the mechanical strain S are usually put in relation with the electric field E and the electric displacement D by means of the following system of tensorial equations

$$\begin{cases} \tilde{T}_i &= \tilde{c}^{\mathrm{D}}_{ij}\tilde{S}_j - \tilde{h}_{iq}\tilde{D}_q \qquad i,j = 1,\dots,6 \\ \tilde{E}_p &= -\tilde{h}_{pj}\tilde{S}_j + \tilde{\beta}^{\mathrm{S}}_{pq}\tilde{D}_q \qquad p,q = 1,\dots,3 \end{cases}, \tag{1}$$

where $\tilde{T}$ and $\tilde{S}$ are rank-2 tensors expressed in reduced index form [30], [32], $\tilde{E}$ and $\tilde{D}$ are rank-1 tensors, whereas $\tilde{c}$, $\tilde{\beta}$, and $\tilde{h}$ are the rank-2 tensors related to mechanical stiffness, dielectric impermittivity, and piezoelectric constant, respectively. Moreover, superscript "D" indicates that the elastic stiffness is computed at constant D, while superscript "S" indicates that the dielectric impermittivity is computed at constant S.

Figure 1 shows a piezoelectric plate poled and excited along the z-axis. If the thickness d is much smaller than both the length l and the width w, the hypothesis of thickness-mode is valid, and (1) reduces to a system of scalar equations [32]. In audio applications, two modes of motion are typically considered: 33-mode and 31-mode [42]. In this work, we concentrate on 33-mode only: we assume an out-of-plane strain, and we consider the PE plate radiating parallel to the poling axis. It follows that (1) can be simplified as

$$\begin{cases} T_3(t) &= c^{\mathrm{D}}_{33}S_3(t) - h_{33}D_3(t) \\ E_3(t) &= -h_{33}S_3(t) + \beta^{\mathrm{S}}_{33}D_3(t) \end{cases}, \tag{2}$$

where the dependence on the time variable t is made explicit, and all the physical components but the ones with index number 3 are considered to be negligible. If the application requires to take into account other modes of motion, (2) will change accordingly, showing different physical and tensorial components [32]. It is thus straightforward to apply the analysis presented in the following to other piezo operations.

Equation (2) represents the starting point for the derivation of all the models shown in this paper. In the next section, we provide, instead, background knowledge on WDFs that will be fundamental further ahead for designing discrete-time implementations of PE transducers.

III. Background on Wave Digital Filters

In traditional WDF theory [16], each circuit element is turned into a WD block characterized by a port-wise description: each port voltage V and port current I is related to an incident wave a and a reflected wave b according to a linear transformation of variables in the form

$$a = V + ZI\,, \qquad b = V - ZI\,, \tag{3}$$

where the free parameter Z is called *port resistance*. Provided that $Z \neq 0$, the inverse mapping of (3) is

$$V = \frac{a+b}{2}\,, \qquad I = \frac{a-b}{2Z}\,. \tag{4}$$

The free parameter Z is usually set to eliminate the local instantaneous dependence of b on a [16]. However, this process, which is called *adaptation*, can be carried out only for a class of linear elements. In all the other cases, iterative procedures are usually required to eliminate *delay-free-loops* [22], [23], [26], [27].

A. Linear Elements

Being V the port voltage, I the port current, R_{g} a resistive parameter, and V_{g} a voltage parameter, a large group of linear one-port elements can be described in the discrete-time domain by the following Thévenin model

$$V[k] = R_{\mathrm{g}}[k]I[k] + V_{\mathrm{g}}[k]\,, \tag{5}$$

where k is the sampling index. As discussed in [18], eq. (5) is able to describe not only resistors and resistive sources, but also dynamic elements such as inductors and capacitors. A general WD realization of such a Thévenin model can be derived substituting (4) into (5) by obtaining

$$b[k] = \frac{R_{\mathrm{g}}[k] - Z[k]}{R_{\mathrm{g}}[k] + Z[k]}a[k] + \frac{2Z[k]}{R_{\mathrm{g}}[k] + Z[k]}V_{\mathrm{g}}[k]\,. \tag{6}$$

The adaptation condition that leads to the elimination of the instantaneous dependence of $b[k]$ on $a[k]$ is $Z = R_{\mathrm{g}}[k]$. If this holds true, eq. (6) reduces to $b[k] = V_{\mathrm{g}}[k]$.

B. Topological Connection Networks

The scattering relation of WD N-port junctions, which model the topological interconnections among elements, can be expressed in matrix form as

$$\mathbf{b} = \mathbf{S}\mathbf{a}\,, \tag{7}$$

where $\mathbf{b} = [b_1,\dots,b_{\mathrm{N}}]^{\mathrm{T}}$ is the vector of waves reflected by the junction, $\mathbf{a} = [a_1,\dots,a_{\mathrm{N}}]^{\mathrm{T}}$ is the vector of waves incident to the junction, and $\mathbf{S}$ is a $N \times N$ scattering matrix. Being $\mathbf{Z}$ a diagonal matrix with port resistances as non-zero entries, the vector of port voltages $\mathbf{v} = [V_1,\dots,V_N]^{\mathrm{T}}$ and the vector of port currents $\mathbf{i} = [I_1,\dots,I_N]^{\mathrm{T}}$ can be evaluated applying $\mathbf{v} = \frac{1}{2}(\mathbf{a}+\mathbf{b})$ and $\mathbf{i} = \frac{1}{2}\mathbf{Z}^{-1}(\mathbf{a}-\mathbf{b})$, respectively. Given that the circuit topology of a reciprocal lossless network is completely described by the fundamental cut-set matrix $\mathbf{Q}$ (of size $\chi \times N$) or the fundamental loop matrix $\mathbf{B}$ (of size $\psi \times N$) [43], [44], matrix $\mathbf{S}$ can be assessed exploiting one of two dual formulas [45], [46]

$$\mathbf{S} = 2\mathbf{Q}^{\mathrm{T}}(\mathbf{Q}\mathbf{Z}^{-1}\mathbf{Q}^{\mathrm{T}})^{-1}\mathbf{Q}\mathbf{Z}^{-1} - \mathbf{I}\,, \tag{8}$$

$$\mathbf{S} = \mathbf{I} - 2\mathbf{Z}\mathbf{B}^{\mathrm{T}}(\mathbf{B}\mathbf{Z}\mathbf{B}^{\mathrm{T}})^{-1}\mathbf{B}\,, \tag{9}$$

where $\mathbf{I}$ is the $N \times N$ identity matrix. Matrices $\mathbf{Q}$ and $\mathbf{B}$ are typically computed starting from a tree-cotree decomposition of the reference circuit [47].

It is worth noticing that, depending on the size of $\mathbf{Q}$ and $\mathbf{B}$, eq. (8) can be more computationally demanding than (9) or vice versa. In particular, if $\chi > \psi$ (9) is cheaper than (8), whereas if $\chi < \psi$ the opposite holds true.

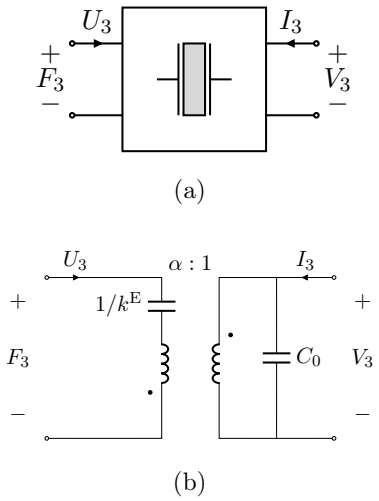

Fig. 2. Under the hypothesis of quasi-static regime and considering one mechanical boundary fixed in space, the piezo can be seen has a two-port element having one mechanical port and one electrical port (a). Exploiting the force-voltage analogy, it is possible to derive a lumped circuital description of such a PE system (b).

IV. Lumped Models of Piezoelectric Transducers

The purpose of lumped models is simplifying as much as possible the physical systems under consideration without significantly impairing the accuracy of the representation. Among lumped models, in this work, we are interested in deriving circuital representations of the reference physical systems. The system of equations (2) describes the linear behavior of piezoelectric transducers as a function of the so called *local state variables*, i.e., mechanical stress T, mechanical strain S, electrical field E, and electrical displacement D. As shown in the following, by employing linear integro-differential relations, it is possible to express (2) as a function of *global state variables* (physical quantities that can be directly measured), i.e., force, velocity, voltage, and current, thus obtaining a circuital lumped model.

If the frequencies of the signals into play are much lower than the first resonant mode frequency of the piezo itself, we can consider the transducer as operating in *quasi-static regime*, meaning that T and S can be regarded as constant along the PE plate [12], [31]. Hence, the mechanical displacement X can be considered the same for each point of the PE system [31]. Moreover, we assume the piezo to be fixed in space at one of its mechanical boundaries, as it happens in many audio applications. It follows that X can be described by a single coordinate. The charge flow, instead, can be evaluated by integrating the electric displacement on the electrode surfaces.

In order to accomplish such a reformulation, let us first rewrite the system of equations (2) as a function of the electric field E

$$\begin{cases} T_3(t) &= c_{33}^{\mathrm{E}} S_3(t) - e_{33} E_3(t) \\ D_3(t) &= e_{33} S_3(t) + \varepsilon_{33}^{\mathrm{S}} E_3(t) \end{cases}, \tag{10}$$

where $e_{33} = h_{33}\varepsilon_{33}^{\mathrm{S}} = h_{33}/\beta_{33}^{\mathrm{S}}$ is a piezoelectric constant, whereas $c^{\mathrm{E}} = c^{\mathrm{D}} - h_{33}e_{33}$ is the mechanical stiffness at

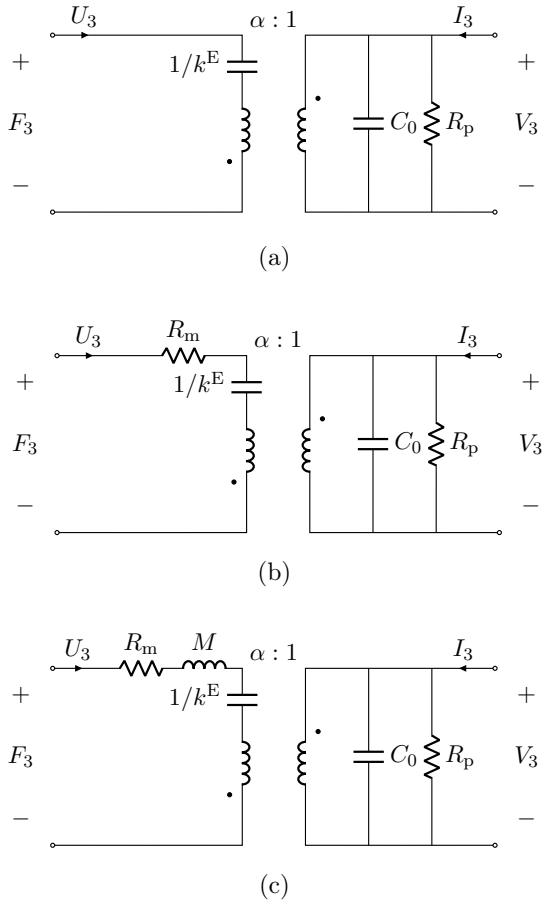

Fig. 3. Different lumped models of PE transducers. (a) Resistive parameter $\boldsymbol{R}_{\mathrm{p}}$ considered at the electric port; (b) Disspative parameter $\boldsymbol{R}_{\mathrm{m}}$ added at the mechanical port; (c) Mass $\boldsymbol{M}$ of the PE transducer added at the mechanical port.

constant E. We can then express (10) in terms of strain S, force F, displacement X, voltage V, and electric charge Q obtaining

$$\begin{cases} F_3(t) &= k^{\mathrm{E}} X_3(t) - \alpha V_3(t) \\ Q_3(t) &= \alpha S_3(t) + C_0 V_3(t) \end{cases}, \tag{11}$$

where $k^{\mathrm{E}} = c_{33}^{\mathrm{E}} lw/d$ is the elastic stiffness, $\alpha = e_{33}lw/d$ represents an electromechanical transduction factor, and $C_0 = \varepsilon_{33}^{\mathrm{S}} lw/d$ is the so-called *static capacitance* (or *clamped capacitance*) [32]. Finally, by recasting the first equation as a function of velocity U and differentiating the second, the quasi-static piezoelectric transducer can be described in the frequency domain by

$$\begin{cases} \mathcal{F}_3(\omega) &= \frac{k^{\mathrm{E}}}{\jmath\omega}\mathcal{U}_3(\omega) - \alpha\mathcal{V}_3(\omega) \\ \mathcal{I}_3(\omega) &= \alpha\mathcal{U}_3(\omega) + \jmath\omega C_0 \mathcal{V}_3(\omega) \end{cases}, \tag{12}$$

where $\mathcal{I}_3$ is the electric current at the transducer electric port.[1] Piezos can be thus seen as two-port elements, having one mechanical port (featuring force F_3 and velocity U_3) and one electrical port (featuring voltage V_3 and current I_3), as shown

[1]Note that, throughout the whole manuscript, we will use calligraphic font, e.g., $\mathcal{I}_3$, for frequency-domain variables and italic font, e.g., I_3, for time-domain variables.

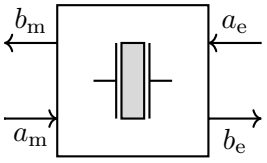

Fig. 4. Piezoelectric transducer modeled as a two-port in the Wave Digital domain.

in Fig. 2(a). Moreover, force/voltage and velocity/current are not only global variables but also *across* and *through* variables, respectively, i.e., variables whose product gives a power. This will come in handy for the derivation of WD implementations of PE transducers, since such a choice allows us to represent these multiphysics systems via a circuital equivalent. In fact, by exploiting the common force-voltage analogy [31], it is possible to derive the equivalent circuit shown in Fig. 2(b), where the electromechanical transduction is represented by an ideal transformer with turn ratio α (i.e., the electromechanical transduction factor). In order to make the model compliant with physical evidences, it is possible to add specific components at the two ports. For instance, it is possible to take into account the non-ideal insulating property of PE materials by considering a finite (but yet very high) conductivity adding resistor R_p in parallel to the electrical port, as shown in Fig. 3(a). Equation (12) can be thus reformulated as follows

$$\begin{cases} \mathcal{F}_3(\omega) &= \frac{k^\mathrm{E}}{\jmath\omega}\mathcal{U}_3(\omega) - \alpha\mathcal{V}_3(\omega) \\ \mathcal{I}_3(\omega) &= \alpha\,\mathcal{U}_3(\omega) + \left(\jmath\omega C_0 + \frac{1}{R_\mathrm{p}}\right)\mathcal{V}_3(\omega) \end{cases}, \tag{13}$$

whereas, whether also a dissipative parameter R_m is taken into account at the mechanical port, it can be rewritten as

$$\begin{cases} \mathcal{F}_3(\omega) &= \left(\frac{k^\mathrm{E}}{\jmath\omega} + R_\mathrm{m}\right)\mathcal{U}_3(\omega) - \alpha\mathcal{V}_3(\omega) \\ \mathcal{I}_3(\omega) &= \alpha\,\mathcal{U}_3(\omega) + \left(\jmath\omega C_0 + \frac{1}{R_\mathrm{p}}\right)\mathcal{V}_3(\omega) \end{cases}. \tag{14}$$

The circuital representation of (14) is shown in Fig. 3(b). As discussed in [12], it is possible to describe the behavior of a PE transducer up to or at least just beyond its first resonant mode, by adding to the model the mass M of the piezo itself. In this case, the piezo can be represented by means of the circuit shown in Fig. 3(c) and its constitutive equations become

$$\begin{cases} \mathcal{F}_3(\omega) &= \left(\frac{k^\mathrm{E}}{\jmath\omega} + R_\mathrm{m} + \jmath\omega M\right)\mathcal{U}_3(\omega) - \alpha\mathcal{V}_3(\omega) \\ \mathcal{I}_3(\omega) &= \alpha\,\mathcal{U}_3(\omega) + \left(\jmath\omega C_0 + \frac{1}{R_\mathrm{p}}\right)\mathcal{V}_3(\omega) \end{cases}. \tag{15}$$

Finally, it is worth highlighting that the models derived in this section take into account both the electrical and mechanical domains but not the acoustic domain since it is not directly involved in the transduction. The acoustic domain can, however, be modeled in a separate fashion, following for example the approach in [48], and then coupled to the PE equivalent circuit through its mechanical port.

A. WD Implementation of PE Lumped Models

Let us now derive the foregoing quasi-static models in the WD domain. Waves relative to the electrical port will be marked with subscript "e," whereas waves relative to the mechanical port will be marked with subscript "m," as shown in Fig. 4. Employing across and through variables allows us to directly apply the inverse mapping shown in (4). We can express, in fact, the Kirchhoff variables F_3, U_3, V_3, and I_3 as functions of the wave variables a_m, b_m, a_e, and b_e as

$$\begin{aligned} F_3(t) &= \tfrac{1}{2}(a_\mathrm{m}(t) + b_\mathrm{m}(t))\,, \quad U_3(t) = \tfrac{1}{2Z_\mathrm{m}(t)}(a_\mathrm{m}(t) - b_\mathrm{m}(t))\,, \\ V_3(t) &= \tfrac{1}{2}(a_\mathrm{e}(t) + b_\mathrm{e}(t))\,, \quad I_3(t) = \tfrac{1}{2Z_\mathrm{e}(t)}(a_\mathrm{e}(t) - b_\mathrm{e}(t))\,, \end{aligned} \tag{16}$$

where Z_m and Z_e are the free parameters referred to mechanical and electrical ports, respectively. By employing Backward Euler as discretization method and substituting (16) in the discrete-time version of (12), a possible WD realization is

$$\begin{bmatrix} b_\mathrm{e}[k] \\ b_\mathrm{m}[k] \end{bmatrix} = \mathbf{S_{PE}} \begin{bmatrix} a_\mathrm{e}[k] \\ a_\mathrm{m}[k] \end{bmatrix} + \mathbf{P_{PE}} \begin{bmatrix} a_\mathrm{e}[k-1] \\ a_\mathrm{m}[k-1] \end{bmatrix} + X_3[k-1]\mathbf{D_{PE}}\,, \tag{17}$$

where k is the sampling index such that, for example, $a_\mathrm{e}[k] = a_\mathrm{e}(kT_\mathrm{s})$ and T_s is the sampling period. Variable X_3 can be computed as

$$X_3[k-1] = X_3[k-2] + \frac{T_\mathrm{s}}{2Z_\mathrm{m}[k-1]}\left(a_\mathrm{m}[k-1] - b_\mathrm{m}[k-1]\right) \tag{18}$$

and it is the integral of velocity U_3, whose use allows us to simplify the WD representation. Moreover, in (17) scattering matrix $\mathbf{S_{PE}}$, matrix $\mathbf{P_{PE}}$, and vector $\mathbf{D_{PE}}$ are defined as

$$\mathbf{S_{PE}} = \begin{bmatrix} -\frac{\beta_3}{\beta_2} & \left[\frac{\gamma - Z_\mathrm{m}[k]}{\alpha Z_\mathrm{m}[k]}\left(\frac{\beta_3\beta_1}{2\beta_2} - \frac{\beta_1 - 2}{2}\right) + \frac{\alpha Z_\mathrm{e}[k]}{Z_\mathrm{m}[k]}\left(\frac{\beta_3}{2\beta_2} - \frac{1}{2}\right)\right] \\ -\frac{2}{\beta_2} & \frac{1}{\beta_2}\left[\beta_1\frac{\gamma - Z_\mathrm{m}[k]}{\alpha Z_\mathrm{m}[k]} + \frac{\alpha Z_\mathrm{e}[k]}{Z_\mathrm{m}[k]}\right] \end{bmatrix},$$

$$\mathbf{P_{PE}} = \begin{bmatrix} \frac{C_0 Z_\mathrm{e}[k]}{T_\mathrm{s}}\left(\frac{1}{2} - \frac{\beta_3}{2\beta_2}\right) & \frac{C_0 Z_\mathrm{e}[k]}{T_\mathrm{s}}\left(\frac{1}{2} - \frac{\beta_3}{2\beta_2}\right) \\ -\frac{C_0 Z_\mathrm{e}[k]}{T_\mathrm{s}\beta_2} & -\frac{C_0 Z_\mathrm{e}[k]}{T_\mathrm{s}\beta_2} \end{bmatrix},$$

$$\mathbf{D_{PE}} = \begin{bmatrix} \frac{k^\mathrm{E}}{\alpha}\left(\frac{\beta_1\beta_3}{\beta_2} - (\beta_1 - 2)\right) \\ \frac{2k^\mathrm{E}\beta_1}{\alpha\beta_2} \end{bmatrix},$$

where

$$\begin{aligned} \gamma &= k^\mathrm{E}T_\mathrm{s}\,, \\ \beta_1 &= 1 + \frac{C_0 Z_\mathrm{e}[k]}{T_\mathrm{s}}\,, \\ \beta_2 &= \beta_1\frac{\gamma + Z_\mathrm{m}[k]}{\alpha Z_\mathrm{m}[k]} + \frac{\alpha Z_\mathrm{e}[k]}{Z_\mathrm{m}[k]}\,, \\ \beta_3 &= (\beta_1 - 2)\frac{\gamma + Z_\mathrm{m}[k]}{\alpha Z_\mathrm{m}[k]} + \frac{\alpha Z_\mathrm{e}[k]}{Z_\mathrm{m}[k]}\,. \end{aligned} \tag{19}$$

We can consider parameter γ as the one describing the mechanical port, whereas parameter β_1 as the one describing the electrical port. Such a parametrization is very useful, since it allows us to change model just by changing γ and/or β_1 according to which port is modified. In fact, the realization of (13) in the WD domain is obtained by setting

$$\beta_1 = 1 + Z_\mathrm{e}[k]\left(\frac{C_0}{T_\mathrm{s}} + \frac{1}{R_\mathrm{p}}\right)\,, \tag{20}$$

and considering (17) for the computation of the reflected waves. Instead, if the specific PE transducer is characterized by a non-negligible dissipative term at the mechanical port (see (14)), the only additional action to be performed is setting

$$\gamma = k^{\mathrm{E}} T_{\mathrm{s}} + R_{\mathrm{m}} \,. \tag{21}$$

Finally, when the application requires to operate the piezo up to or at least around its first resonant mode, we need to take into account the mass of the transducer [12] (see (15)). This can be done in the WD domain by setting

$$\gamma = k^{\mathrm{E}} T_{\mathrm{s}} + \frac{M}{T_{\mathrm{s}}} + R_{\mathrm{m}} \,, \tag{22}$$

and by modifying (17) as

$$\begin{aligned} \begin{bmatrix} b_{\mathrm{e}}[k] \\ b_{\mathrm{m}}[k] \end{bmatrix} = \mathbf{S_{PE}} \begin{bmatrix} a_{\mathrm{e}}[k] \\ a_{\mathrm{m}}[k] \end{bmatrix} + \mathbf{P_{PE}} \begin{bmatrix} a_{\mathrm{e}}[k-1] \\ a_{\mathrm{m}}[k-1] \end{bmatrix} + \\ + \mathbf{M_{PE}} \begin{bmatrix} a_{\mathrm{m}}[k-1] \\ b_{\mathrm{m}}[k-1] \end{bmatrix} + X_3[k-1] \mathbf{D_{PE}} \,, \end{aligned} \tag{23}$$

in order to account for the derivative operation associated with mass M (see (15)). The only difference between (17) and (23) is thus the presence of

$$\mathbf{M_{PE}} = \begin{bmatrix} \frac{-M}{2\alpha T_{\mathrm{s}} Z_{\mathrm{m}}[k-1]} \left(\frac{\beta_3 \beta_1}{2\beta_2} - \frac{\beta_1 - 2}{2} \right) & \frac{M}{2\alpha T_{\mathrm{s}} Z_{\mathrm{m}}[k-1]} \left(\frac{\beta_3 \beta_1}{2\beta_2} - \frac{\beta_1 - 2}{2} \right) \\ \frac{-M}{2\alpha T_{\mathrm{s}} Z_{\mathrm{m}}[k-1]} \frac{\beta_1}{\beta_2} & \frac{-M}{2\alpha T_{\mathrm{s}} Z_{\mathrm{m}}[k-1]} \frac{\beta_1}{\beta_2} \end{bmatrix},$$

which weighs past samples of incident and reflected waves at the transducer mechanical port.

Once the best suited model for the application is chosen, not only it is possible to efficiently simulate it, but also to integrate it into more complex WD structures [24], [37]. In this case, it is desirable to remove as much as possible the implicit relations that take place when WD blocks are connected. In other words, we would like to remove the instantaneous dependences between reflected and incident waves such that delay-free-loops are eliminated. We do this by deriving adaptation conditions specific to the presented WD realizations of PE transducers. Given that all the models derived in this section share the same scattering matrix $\mathbf{S_{PE}}$, the adaptation conditions will be the same as well. By setting to zero the first diagonal entry of $\mathbf{S_{PE}}$ and by solving for Z_{e}, we obtain the following adaptation condition for the electrical port

$$Z_{\mathrm{e}}[k] = \frac{\gamma + Z_{\mathrm{m}}[k]}{\alpha^2 + \frac{\beta_1 - 1}{Z_{\mathrm{e}}[k]} \left(\gamma + Z_{\mathrm{m}}[k] \right)} \,, \tag{24}$$

whereas the adaptation condition for the mechanical port can be obtained by setting to zero the second diagonal entry of $\mathbf{S_{PE}}$ and solving for Z_{m} as

$$Z_{\mathrm{m}}[k] = \frac{\alpha^2 Z_{\mathrm{e}}[k]}{\beta_1} + \gamma \,. \tag{25}$$

It is worth noticing that (24) and (25) are functions of γ and β_1 and thus they account for variations at both electrical and mechanical ports.

The proposed implementations of PE transducers are only some of the many; it is possible, for example, to employ the traditional theory of WDFs to derive other equivalent realizations [16]. However, we decided to pursue the proposed approach aiming at a more compact representation, defining at the same time a practical parametrization.

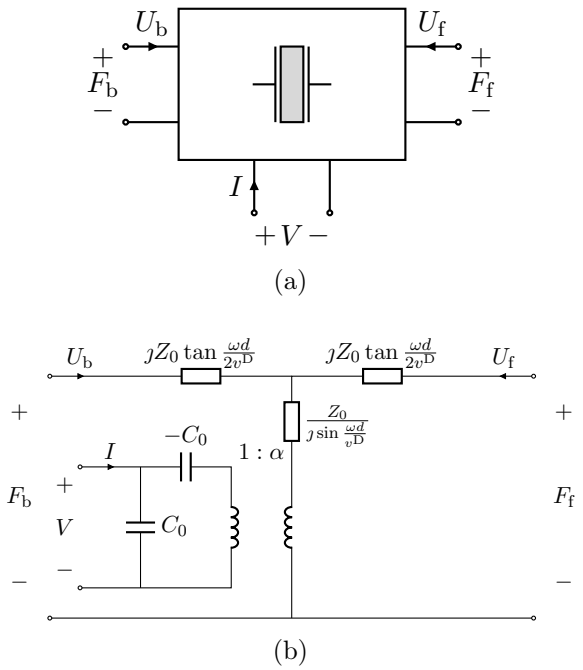

Fig. 5. Piezoelectric transducer modeled as a three-port in the Kirchhoff domain (a), and one of its possible distributed circuital models, known as Mason's model (b) [32]. Subscript "b" stands for "back" port, whereas "f" stands for "front" port.

Finally, this section does not cover all the possible physical models of piezos operating in quasi-static regime (see [31]). Nevertheless, other possible WD implementations can be derived with ease following the same approach proposed in this manuscript.

V. Distributed Model of Piezoelectric Transducers

In the previous section, we derived lumped models suitable to describe operations in quasi-static regime, i.e., with frequencies much lower than the first resonant mode frequency of the piezo itself. However, when it is necessary to operate the device at frequencies greater than the first resonant mode frequency, the hypothesis of quasi-static regime is no longer valid (T and S cannot be considered constant anymore), meaning that the propagation of acoustic waves inside the PE plate must be taken into account [32]. In this scenario, displacement X_3 in (2) is governed by the equation describing the propagation of waves inside anisotropic media (such as PE materials) [32]. Nevertheless, considering a uniform medium and that, in the majority of the cases, only purely longitudinal/shear acoustic waves take place, the equation governing X_3 reduces to

$$\frac{\partial^2 X_3(z,t)}{\partial t^2} = v^{\mathrm{D}^2} \frac{\partial^2 X_3(z,t)}{\partial z^2} \,, \tag{26}$$

i.e., the D'Alembert's wave equation, where $v^{\mathrm{D}} = \sqrt{c_{33}^{\mathrm{D}} / \rho}$ is the velocity of propagation at constant D and ρ is the medium density. With the purpose of deriving a more general model, let us consider the PE transducer having unclamped surfaces.

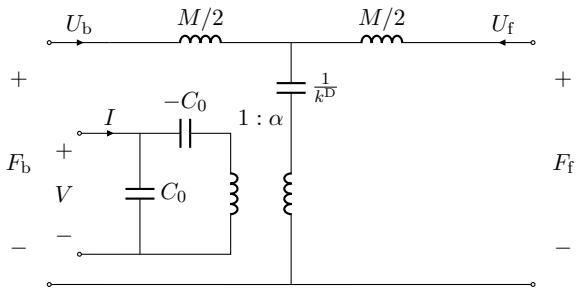

Fig. 6. Linearized version of Mason's model, where the three frequency-dependent components are substituted with two inductors and a capacitor.

Thereby, it can be seen as a component having two mechanical ports and one electrical port, as shown in Fig. 5(a). Assuming an harmonic driving signal $D = D_0 e^{\jmath\omega t}$, (2) can be finally rewritten in the frequency domain as [32]

$$\begin{cases} \mathcal{F}_\mathrm{b}(\omega) = \frac{Z_0}{\jmath \tan \frac{\omega d}{v^\mathrm{D}}} \mathcal{U}_\mathrm{b}(\omega) + \frac{Z_0}{\jmath \sin \frac{\omega d}{v^\mathrm{D}}} \mathcal{U}_\mathrm{f}(\omega) + \frac{h_{33}}{\jmath\omega} \mathcal{I}(\omega) \\ \mathcal{F}_\mathrm{f}(\omega) = \frac{Z_0}{\jmath \sin \frac{\omega d}{v^\mathrm{D}}} \mathcal{U}_\mathrm{b}(\omega) + \frac{Z_0}{\jmath \tan \frac{\omega d}{v^\mathrm{D}}} \mathcal{U}_\mathrm{f}(\omega) + \frac{h_{33}}{\jmath\omega} \mathcal{I}(\omega) \\ \mathcal{V}(\omega) = \frac{h_{33}}{\jmath\omega} \mathcal{U}_\mathrm{b}(\omega) + \frac{h_{33}}{\jmath\omega} \mathcal{U}_\mathrm{f}(\omega) + \frac{1}{\jmath\omega C_0} \mathcal{I}(\omega) \end{cases}, \tag{27}$$

where $Z_0 = \rho l w v^\mathrm{D}$ is the piezo mechanical impedance, $\mathcal{F}_\mathrm{b}$ and $\mathcal{U}_\mathrm{b}$ are the force and the velocity at the back mechanical port, $\mathcal{F}_\mathrm{f}$ and $\mathcal{U}_\mathrm{f}$ are the force and the velocity at the front mechanical port, whereas $\mathcal{V}$ and $\mathcal{I}$ are the voltage and the current at the electric port, respectively.

We introduce now a lumped representation of the distributed model in (27). In particular, Fig. 5(b) shows a circuital representation of (27) known under the name of Mason's model [32]. The peculiarities of such a model are the three two-terminal elements represented as rectangles in Fig. 5(b), which, varying in a nonlinear fashion with frequency, act as delay lines and model the propagation inside the medium. Such elements cannot be implemented in mainstream circuit analysis programs and, therefore, they are usually substituted with transmission lines in order to replicate their distributed nature [49], [50]. In the following, instead, we show how it is possible to implement them in the WD domain for time-domain analyses.

A. WD Mason's Model: Linearized Model

A first and simplified WD realization of Mason's model is based on the following mathematical considerations. Tangent function $\tan x$ and sine function $\sin x$ can be approximated with their argument x if x is close to zero. Naming $T_\mathrm{t} = d/v^\mathrm{D}$ the plate-to-plate transit time along z-axis, we can simplify the constitutive relation of the frequency-dependent elements as follows

$$\jmath Z_0 \tan \frac{\omega T_\mathrm{t}}{2} \underset{\frac{\omega T_\mathrm{t}}{2} \to 0}{\approx} \jmath\omega \frac{Z_0 T_\mathrm{t}}{2} = \jmath\omega L \,, \tag{28}$$

where

$$L = \frac{Z_0 T_\mathrm{t}}{2} = \rho \frac{lwd}{2} = \frac{M}{2} \,, \tag{29}$$

for the element characterized by the tangent function (hereafter indicated with $\jmath\tan$ element), whereas

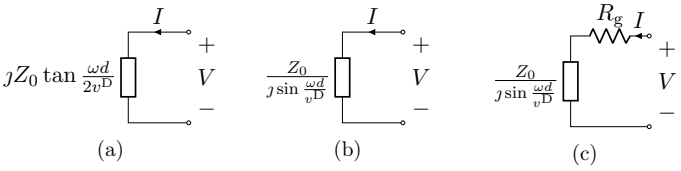

Fig. 7. (a) Constitutive relation of the $\jmath\tan$ element shown in Fig. 5; (b) constitutive relation of the $\jmath\sin$ element shown in Fig. 5, which, once modeled in the WD domain, cannot be adapted; (c) modified $\jmath\sin$ element, which thanks to a the resistive parameter R_g, once modeled in the WD domain, can be adapted.

$$\frac{Z_0}{\jmath \sin \omega T_\mathrm{t}} \underset{\omega T_\mathrm{t} \to 0}{\approx} \frac{1}{\jmath\omega \frac{T_\mathrm{t}}{Z_0}} = \frac{1}{\jmath\omega C} \,, \tag{30}$$

where

$$C = \frac{T_\mathrm{t}}{Z_0} = \frac{d}{lwc_{33}^\mathrm{D}} = \frac{1}{k^\mathrm{D}} \,, \tag{31}$$

for the element characterized by the sine function (hereafter indicated with $\jmath\sin$ element). As a result, the linearized version of Mason's model (shown in Fig. 6) features only dynamic components, where the relation with frequency is made explicit. In particular, $\jmath\tan$ is substituted with an inductor whose inductance is equal to half the transducer mass, while $\jmath\sin$ is substituted with a capacitor whose capacitance is the inverse of k^D, i.e., the elastic stiffness at constant D.

It is worth noticing that such a linearized model maintains an evident physical meaning, since inductance L and capacitance C are strictly dependent on the physical/geometrical properties of the PE transducers. Moreover, the choice of employing the proposed approach strictly depends on the product between the angular frequency into play ω and the transit time T_t (as shown in (28) and (30)), a product that can be easily computed *a priori* considering the upper limit of the audio bandwidth (e.g., 20 kHz).

Finally, the WD implementation of the circuit shown in Fig. 6 is obtained by applying the WDF principles summarized in Section III.

B. WD Mason's Model: Frequency-Dependent Model

Since the hypotheses of linearization used in the previous subsection might not always be valid, a method for the WD implementation of those elements characterized by nonlinear functions of frequency is necessary. Our purpose is thus to find their WD scattering relations. What makes the implementation of such elements tricky is their implicit dependence on ω, which does not allow a straightforward discretization in the time domain. In fact, we usually deal with inductors or capacitors, for which the aforementioned dependence is explicit, and thus common discretization methods (e.g., Backward Euler, trapezoidal rule, etc.) can be employed. We can, however, sort this problem out by applying Euler's formulas as explained in the following.

Let us first consider the two-terminal $\jmath\tan$ element shown in Fig. 7(a). By applying Euler's tangent formula, we can rewrite

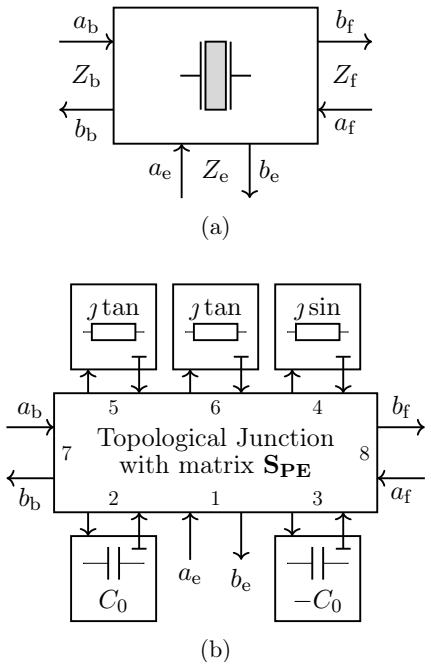

Fig. 8. (a) PE transducer in the WD domain. Subscripts "b," "f," and "e" refers to the waves at the back mechanical, front mechanical, and electrical ports, respectively; (b) possible WD realization of such a three-port element.

its constitutive equation as

$$\mathcal{V}(\omega) = \jmath Z_0 \tan\frac{\omega d}{2v^\mathrm{D}}\mathcal{I}(\omega) = Z_0\frac{1-e^{-\jmath\omega T_\mathrm{t}}}{1+e^{-\jmath\omega T_\mathrm{t}}}\mathcal{I}(\omega)\,, \tag{32}$$

and, by applying the *starred transform* [51], we can then write it in the Z-domain

$$\mathcal{V}(z) = Z_0\frac{1-z^{-T}}{1+z^{-T}}\mathcal{I}(z)\,, \tag{33}$$

where, for simplicity, $T = T_\mathrm{t}/T_\mathrm{s}$ is assumed to be an integer number and T_s is the sampling time. It follows that, according to the aforementioned assumption, T_s must be chosen to be a submultiple of T_t. The discrete-time version of (33) is $V[k] = Z_0 I[k] - Z_0 I[k-T] - V[k-T]$, which, once applied the linear transformation of variables shown in (3), gives finally place to the pursed scattering relation

$$b[k] = \frac{Z_0 - Z}{Z_0 + Z}a[k] - a[k-T] + \frac{Z_0 - Z}{Z_0 + Z}b[k-T]\,. \tag{34}$$

Moreover, by setting $Z = Z_0$ we can *adapt* the element and eliminate the instantaneous dependence of $b[k]$ from $a[k]$. The scattering relation, therefore, reduces to $b[k] = -a[k-T]$. Such a result is interesting since, if we consider $T = 1$, we obtain the scattering relation of an adapted inductor discretized by means of the trapezoidal rule [18], which is exactly the circuit element approximating the $\jmath\tan$ element in the linearized model. In case of adaptation, such a frequency-dependent element is thus modeled in the WD domain as a sign inversion and a delay of T samples, whose value is in turn dependent on the plate-to-plate transit time.

Similar considerations can be drawn for the $\jmath\sin$ element shown in Fig. 7(b). In fact, by applying Euler's sine formula we can rewrite its constitutive equation as

$$\mathcal{V}(\omega) = \frac{Z_0}{\jmath\sin\frac{\omega d}{v^\mathrm{D}}}\mathcal{I}(\omega) = \frac{2Z_0 e^{-\jmath\omega T_\mathrm{t}}}{1-e^{-\jmath\omega 2T_\mathrm{t}}}\mathcal{I}(\omega)\,, \tag{35}$$

from which we can easily derive

$$V[k] = 2Z_0 I[k-T] + V[k-2T]\,, \tag{36}$$

and subsequently

$$b[k] = -a[k] + \frac{2Z_0}{Z}\big(a[k-T] - b[k-T]\big) + a[k-2T] + b[k-2T]\,. \tag{37}$$

Given that in (37) the coefficient of $a[k]$ does not depend on port resistance Z, the scattering relation cannot be adapted. However, as frequently done in WDF modeling [52], it is possible to consider a small series resistance such that the dependence on Z is established and the one-port can be adapted. Taking into account the modified $\jmath\sin$ element shown in Fig. 7(c), we can write its circuital relation in the discrete-time domain as

$$V[k] = R_\mathrm{g} I[k] + 2Z_0 I[k-T] - R_\mathrm{g} I[k-2T] + V[k-2T]\,, \tag{38}$$

where R_g is the series resistance. If opportunely sized, R_g does modify the equation behavior in a negligible fashion, generating, at the same time, an important advantage in terms of computability. In fact, the resulting element in the WD domain is characterized by the scattering relation

$$\begin{aligned} b[k] = {} & \frac{R_\mathrm{g} - Z}{R_\mathrm{g} + Z}a[k] + \frac{2Z_0}{Z + R_\mathrm{g}}\big(a[k-T] - b[k-T]\big) + \\ & - \frac{R_\mathrm{g} - Z}{R_\mathrm{g} + Z}a[k-2T] + b[k-2T]\,, \end{aligned} \tag{39}$$

which can be finally adapted by imposing $Z = R_\mathrm{g}$. It follows that (39) reduces to $b[k] = \frac{Z_0}{R_\mathrm{g}}\big(a[k-T] - b[k-T]\big) + b[k-2T]$.

Once obtained the scattering relation of the two frequency-dependent one-ports, the PE system shown in Fig. 5(b) can be easily implemented in the WD domain following the principles summarized in Section III. A PE transducer can again be seen as a three-port element (see Fig. 8(a)), whose waves facing the back mechanical port, the front mechanical port, and the electrical port are marked with subscripts "b," "f," and "e," respectively. A possible WD realization is shown, instead, in Fig. 8(b), where the three external ports are highlighted.

It is worth adding that, although setting T_s as a submultiple of T_t allows us to obtain simple and compact scattering relations (avoiding fractional sampling indexes), it constraints at the same time the choice of the sampling frequency $f_\mathrm{s} = 1/T_\mathrm{s}$, which cannot be arbitrarily set. For instance, in order to increase f_s we have to increase $T = T_\mathrm{t}/T_\mathrm{s}$. We do this by setting T_s equal to a lower submultiple of T_t; conversely, we have to lower T. Finally, as far as implementations on Digital Signal Processors (DSPs) are concerned, T is set in order to match as closely as possible the given sampling frequency. In fact, only a few f_s (and thus T_s) are allowed by the DSP. If a perfect correspondence cannot be accomplished, an error in the system response arises. However, such an error can be kept small by a proper tuning of T, or by upsampling/downsampling the input signal in order to match f_s (and

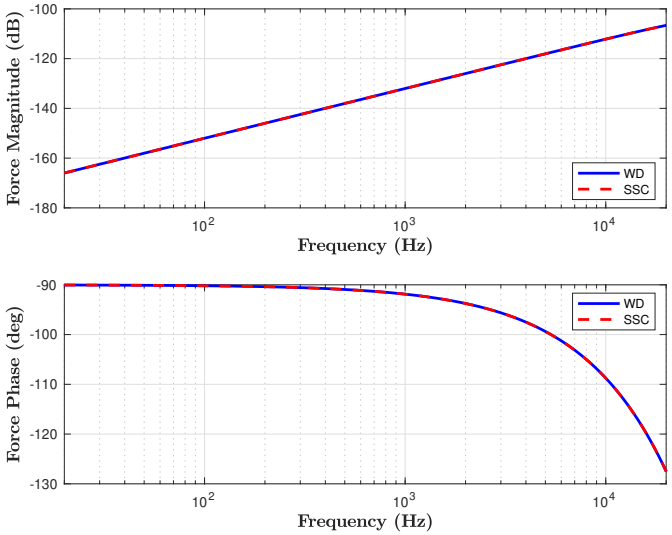

Fig. 9. Magnitude and phase of Force $\boldsymbol{F_3}$ at the transducer mechanical port (see Fig. 3(a)) when loaded with mechanical resistor $\boldsymbol{R_{\text{mecc}} = 0.33}$ kg/s. The continuous blue curve represents the WD implementation, whereas the dashed red curve the MathWorks Simscape (SSC) implementation.

resampling the output signal whenever needed), thus making, in many cases, this disadvantage marginal with respect to the advantage of avoiding fractional sampling indexes and higher computational costs.

Finally, note that the PE equivalent circuit models considered in this manuscript (both lumped and distributed) are only able to describe ideal PE transducers and, therefore, do not take into account nonlinearities (e.g., hysteresis), losses (e.g., piezoelectric, mechanical, etc.), or other nonidealities affecting the transduction process (e.g., duffing, spurious modes, etc.). Nonetheless, in many cases, linear piezoelectric models provide a sufficient degree of accuracy for the characterization of audio systems [42]. Moreover, although all the WDFs obtained in this manuscript are meant to be employed into digital signal processing algorithms for audio applications, the WDFs derived in this section can be also exploited for resonator simulations at higher frequencies, serving thus as tools also for ultrasound applications.

VI. Numerical Examples

In this section, we provide some numerical results obtained by employing the proposed WDF implementations of PE transducers. We take into account both lumped and distributed models. The accuracy of the implementations is confirmed by a comparison whether with MathWorks Simulink or MathWorks Simscape, considering the same fixed sampling step. The modeling of linear elements is addressed following traditional WDF principles; for the specific case of dynamic one-ports, Backward Euler method is chosen for the discretization of the time derivatives characterizing their constitutive equations [18]. Finally, all linear elements are adapted such that the instantaneous relations between wave variables are removed.

A. Lumped Model

For reasons of space, we show the results related to only one of the lumped models proposed in Subsection IV-A, but all of them have been validated through a comparison with a MathWorks Simscape implementation. Let us consider the model shown in Fig. 3(a), where resistor R_{p} is added in parallel to the transducer electrical port in order to take into account its finite conductivity. We consider a $BaTiO_3$ PE plate having as geometric dimensions $d = 0.7$ mm, $w = 20$ mm, and $l = 40$ mm. Moreover, we consider the transducer mechanical port to be loaded with a resistor $R_{\text{mecc}} = 0.33$ kg/s. The remaining parameters are set as follows: $k^{\text{E}} = 0.17$ TN/m, $\alpha = 20$ N/V, $C_0 = 12.7$ nF, and $R_{\text{p}} = 1$ MΩ. The frequency of the first resonant mode can be approximated as

$$f_{\text{r}} \approx \frac{1}{2\pi}\sqrt{\frac{k^{\text{E}}}{M}} = 1.15 \text{ MHz}\,, \tag{40}$$

where the mass M is assessed considering a density $\rho = 5700$ kg/m^3. Hence, being f_{r} much higher than the upper limit of the audio bandwidth, a lumped model is enough to describe the transducer. In order to test the accuracy of the model in (13) over the whole audio spectrum, we perform a frequency analysis computing the Discrete Fourier Transform (DFT) of the discrete-time domain impulse response, where the electrical port is considered as the input port. Figure 9 shows the magnitude and the phase of force F_3 at the transducer mechanical port. The continuous blue curves refer to the WDF, whereas the dashed red curves to MathWorks Simscape (SSC); their good match validates the implementation of the designed WDF.

B. Distributed Model

Let us now consider the more interesting case of the distributed model discussed in Section V. We take into account a ceramic piezo having the following parameters: $d = 0.49$ mm, $w = 10$ mm, $l = 20$ mm, $h_{33} = 79.34$ kV/m, $C_0 = 1$ μF, $\rho = 7750$ kg/m^3, $\alpha = 0.0793$ N/V, $T_{\text{t}} = 0.126$ ms, and $Z_0 = 6.04$ kg/s. The first resonant mode frequency f_{r} is around 3.8 kHz, and thus, being it in the audio bandwidth, a distributed model is necessary to describe the transducer operation. We simulate the circuit shown in Fig. 5(b) by means of the frequency-dependent model derived in Subsection V-B, whose WD realization is shown in Fig. 8(b). We connect to port 7 and port 8 of the WD topological junction two resistors $R_{\text{b}} = R_{\text{f}} = 0.083$ kg/s modeling the mechanical impedances of air, which we consider as the medium facing both back and front surfaces of the PE plate. Then, the transducer can be driven by connecting an input signal to port 1 of the same junction. The three frequency-dependent elements are realized considering the scattering relations derived in Subsection V-B. In particular, as far as the $\jmath\sin$ one-port is concerned, we set $R_{\text{g}} = 1$ $\mu\Omega$. Moreover, we set $T = 20$ such that the sampling step $T_{\text{s}} = T_{\text{t}}/T$ is small enough to avoid aliasing in the audio bandwidth.

In the WD domain, ideal reciprocal lossless elements behaving as connectors, such as ideal transformers, can be encompassed in scattering matrices. Therefore, we decide to

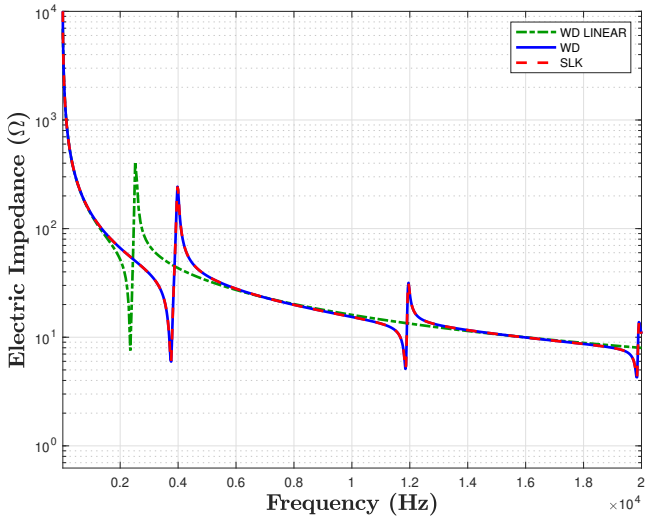

Fig. 10. Impedance at the transducer electric port. The continuous blue curve represents the WD implementation, whereas the dashed red curve the MathWorks Simulink (SLK) implementation. The green dashed curve (WD LINEAR), instead, represents the curve obtained taking into account the linearized Mason's model shown in Fig. 6, and is obtained within MathWorks Simscape.

embed the ideal transformer with turn ratio α into the WD topological junction. Hence, matrix $\mathbf{S_{PE}}$ can be computed by substituting in (9) the fundamental loop matrix

$$\mathbf{B} = \begin{bmatrix} -\alpha & \alpha & 0 & 0 & 0 & 0 & 0 & 0 \\ -\alpha & 0 & -\alpha & -1 & -1 & 0 & 1 & 0 \\ -\alpha & 0 & -\alpha & -1 & 0 & -1 & 0 & 1 \end{bmatrix}, \quad (41)$$

which can be derived starting from the Kirchhoff's current and voltage laws.

In order to test the accuracy of the WD implementation, we perform a frequency analysis of the transducer electric impedance, and we then compare the result with the same curve obtained starting from a block-diagram implementation in MathWork Simulink. In particular, we exploit Euler's formulas in the same way we showed in Subsection V-B for the $\jmath\sin$ and $\jmath\tan$ elements but now applied to the system of equations in (27). Once obtained a discrete-time version of (27), we implement it in Simulink through a block diagram, which, being composed of 88 units, turns out to be very dense. In particular, for processing 10 s, the proposed implementation takes on average (over 100 runs) 5.6 s, while the Simulink implementation takes 1.2 min. Note that it is possible to solve the system of equation e.g., making use of numerical methods such as Newton-Raphson, which may be characterized by a different computational cost. Then, in order to carry out the frequency analysis, we compute the Discrete Fourier Transform of the time-domain impulse response. Figure 10 shows the outcome of such a frequency analysis. The blue and red curves represent the WD and Simulink (SLK) implementations, respectively, whereas the green dashed curve represents the impedance of the linearized Mason's model (see Fig. 6) obtained within MathWorks Simscape. As already pointed out in Subsection V-A, the linearized model can be employed only if the product between the transit time and the frequency into play approaches zero. Looking at the plot, we can verify that such a hypothesis does not hold true already around 2 kHz, and, therefore, a linearized model is not suitable to describe the PE transducer under consideration. On the other hand, the good match between red and blue curves confirms the accuracy of the proposed WDFs.

Finally, it is worth pointing out that the block-based nature of WDFs allows us to connect in cascade with ease several Mason's models [7] for the simulation of multiple layers, accounting thus for different material properties. In addition, WDFs are known to increase the modularity of the representation [16], enabling thus a more straightforward and efficient implementation of these composite structures.

VII. Conclusions

In this paper, we proposed different novel WD implementations of well-known PE models for audio applications. Based on thickness-mode operation, such WDFs are obtained from a circuital representation of the piezo constitutive equations. The models can be mainly divided into two categories: lumped models, which can be applied when the hypotheses for quasi-static regime are satisfied, and distributed models, which take into account the propagation of acoustic waves inside the PE medium. The proposed WD realizations of lumped models are presented as multiphysics two-ports (one electric port and one mechanical port) characterized by scattering relations. Moreover, thanks to the given parametric definition, they can be easily modified to accommodate different elements at the transducer physical ports.

We then showed how it is possible to implement Mason's distributed model in the WD domain. Such a model is usually realized via other equivalent circuits (e.g., Redwood model [49]), since it is not possible to implement its frequency-dependent elements in common Spice-like simulators. Instead, we showed how such one-ports can be realized in the WD domain and how these can be adapted, removing thus the implicit relations between wave variables. Since Mason's model allows us to consider boundary conditions at the transducer surfaces, the proposed WD realization has been presented as a three-port element (two mechanical ports and one electrical port). However, by clamping one of the two mechanical ports, the model can still be described by means of a two-port representation.

Beside such characteristics, the proposed WD models offer other advantages. For example, even when considering stable discretization methods (e.g., Backward Euler), no iterative solvers are required for their solution (i.e., they are explicit), and thanks to their input-output description, they benefit from an enhanced modularity, which comes in handy for the efficient simulation of composite PE structures. Moreover, such WD blocks can be then merged into large nonlinear systems which can be efficiently solved employing the Hierarchical Scattering Iterative Method, recently derived for the simulation of nonlinear multiphysics systems [24], [28], [37]. Most importantly, having digital implementations of piezoelectric transducers in the WD domain paves the way toward the design of algorithms for the linearization/equalization

of the transducer behavior with the aim of enhancing the acoustic performance (e.g., through circuital inversion [38]–[40]). Finally, following the same approach proposed in this paper, other configurations of piezoelectric transducers can be modeled.

Further future work may concern the modeling of piezoelectric losses and nonlinearities, as well as the derivation of temperature-dependent models.

REFERENCES

[1] S. J. Rupitsch, *Piezoelectric Sensors and Actuators: Fundamentals and Applications*. Springer, 2019.

[2] C. Sun, Q. Shi, M. S. Yazici, T. Kobayashi, Y. Liu, and C. Lee, "Investigation of broadband characteristics of multi-frequency piezoelectric micromachined ultrasonic transducer (mf-pmut)," *IEEE Sensors Journal*, vol. 19, pp. 860–867, 2 2019.

[3] E. Vezzoli, Z. Vidrih, V. Giamundo, B. Lemaire-Semail, F. Giraud, T. Rodic, D. Peric, and M. Adams, "Friction reduction through ultrasonic vibration part 1: Modelling intermittent contact," *IEEE Transactions on Haptics*, vol. 10, pp. 196 – 207, 2017.

[4] D. Geng, S. Han, H. Seo, M. Mativenga, and J. Jang, "Piezoelectric pressure sensing device using top-gate effect of dual-gate a-igzo tft," *IEEE Sensors Journal*, vol. 17, pp. 585–586, 2 2017.

[5] C. Peng, M. Chen, H. Wang, J. Shen, and X. Jiang, "Broadband piezoelectric transducers for under-display ultrasonic fingerprint sensing applications," *IEEE Transactions on Industrial Electronics*, vol. 68, pp. 4426–4434, 2020.

[6] R. Subbaramaiah, S. A. Al-Jufout, A. Ahmed, and M. M. Mozumdar, "Design of vibration-sourced piezoelectric harvester for battery-powered smart road sensor systems," *IEEE Sensors Journal*, vol. 20, pp. 13 940–13 949, 12 2020.

[7] V. Shaparov, Z. Sotula, and L. Kunickaya, *Piezo-Electric Electro-Acoustic Transducers*. Springer, 2014.

[8] T. Horikawa and K. Kobayashi, "Application of ceramic piezoelectric device to audio speaker," 8 2008, pp. 1–4.

[9] S. Yuan, S. Huang, X. Chu, and R. Gao, "Optimization methods for acoustic performance of piezoelectric panel loudspeaker," 8 2011, pp. 332–337.

[10] P. Zeng, Y. H. Chen, Y. Y. Gao, Y. P. Li, and G. M. Cheng, "Simulation analysis and experimental research on circular piezoelectric bone-conduction headphone," *Advanced Materials Research*, vol. 1030-1032, pp. 2313–2319, 2014.

[11] X. Li, L. Xu, and L. Xu, "Audio near-distance directional loudspeaker technology for portable multimedia devices," 8 2011, pp. 727–731.

[12] S. A. Prasad, Q. Gallas, S. Horowitz, B. Homeijer, B. V. Sankar, L. N. Cattafesta, and M. Sheplak, "Analytical electroacoustic model of a piezoelectric composite circular plate," *AIAA Journal*, vol. 44, pp. 697–705, 2006.

[13] J. Mendoza-López, S. Sánchez-Solano, and J. L. Huertas-Díaz, "Characterization and modelling of circular piezoelectric micro speakers for audio acoustic actuation," *ISRN Mechanical Engineering*, vol. 2012, p. 635268, 2012.

[14] E. Larsen and R. M. Aarts, *Audio Bandwidth Extension: Application of Psychoacoustics, Signal Processing and Loudspeaker Design*. John Wiley and Sons, Ltd, 2004.

[15] L. K. Chiu, D. V. Anderson, and B. Hoomes, "Audio output enhancement algorithms for piezoelectric loudspeakers," 1 2011, pp. 317–320.

[16] A. Fettweis, "Wave digital filters: Theory and practice," *Proceedings of the IEEE*, vol. 74, pp. 270–327, 1986.

[17] V. Välimäki, F. Fontana, J. O. Smith, and U. Zölzer, "Introduction to the special issue on virtual analog audio effects and musical instruments," *IEEE Transactions on Audio, Speech, and Language Processing*, vol. 18, pp. 713–714, 2010.

[18] A. Bernardini, P. Maffezzoni, and A. Sarti, "Linear multistep discretization methods with variable step-size in nonlinear wave digital structures for virtual analog modeling," *IEEE/ACM Transactions on Audio, Speech, and Language Processing*, vol. 27, pp. 1763–1776, 2019.

[19] A. Fettweis and K. Meerkotter, "On adaptors for wave digital filters," *IEEE Transactions on Acoustics, Speech, and Signal Processing*, vol. 23, pp. 516–525, 12 1975.

[20] A. Sarti and G. D. Sanctis, "Systematic methods for the implementation of nonlinear wave-digital structures," *IEEE Transactions on Circuits and Systems I: Regular Papers*, vol. 56, pp. 460–472, 2009.

[21] G. D. Sanctis and A. Sarti, "Virtual analog modeling in the wave-digital domain," *IEEE Transactions on Audio, Speech, and Language Processing*, vol. 18, pp. 715–727, 2010.

[22] A. Bernardini, P. Maffezzoni, L. Daniel, and A. Sarti, "Wave-based analysis of large nonlinear photovoltaic arrays," *IEEE Transactions on Circuits and Systems I: Regular Papers*, vol. 65, pp. 1363–1376, 2018.

[23] A. Bernardini, E. Bozzo, F. Fontana, and A. Sarti, "A wave digital newton-raphson method for virtual analog modeling of audio circuits with multiple one-port nonlinearities," *IEEE/ACM Transactions on Audio, Speech, and Language Processing*, vol. 29, pp. 2162 – 2173, 2021.

[24] R. Giampiccolo, A. Bernardini, G. Gruosso, P. Maffezzoni, and A. Sarti, "Multiphysics modeling of audio circuits with nonlinear transformers," *Journal of the Audio Engineering Society*, vol. 69, pp. 374–388, 6 2021.

[25] R. Giampiccolo, M. G. de Bari, A. Bernardini, and A. Sarti, "Wave digital modeling and implementation of nonlinear audio circuits with nullors," *IEEE/ACM Transactions on Audio, Speech, and Language Processing*, vol. 29, pp. 3267–3279, 2021.

[26] M. J. Olsen, K. J. Werner, and J. O. Smith, "Resolving grouped nonlinearities in wave digital filters using iterative techniques," 9 2016.

[27] T. Schwerdtfeger and A. Kummert, "A multidimensional approach to wave digital filters with multiple nonlinearities," 9 2014, pp. 2405–2409.

[28] R. Giampiccolo, A. Natoli, A. Bernardini, and A. Sarti, "Parallel wave digital filter implementations of audio circuits with multiple nonlinearities," *AES: Journal of the Audio Engineering Society*, vol. 70, pp. 469–484, 6 2022.

[29] A. Bernardini, A. Sarti, P. Maffezzoni, and L. Daniel, "Wave digital-based variability analysis of electrical mismatch in photovoltaic arrays," in *IEEE International Symposium on Circuits and Systems (ISCAS)*, 5 2018, pp. 1–5.

[30] "Ieee standard on piezoelectricity," *ANSI/IEEE Std 176-1987*, 1987.

[31] B. Richter, J. Twiefel, and J. Wallaschek, "Piezoelectric equivalent circuit models," pp. 107–128, 2009.

[32] D. A. Berlincourt, D. R. Curran, and H. Jaffe, "Piezoelectric and piezomagnetic materials and their function in transducers," pp. 169–270, 1964.

[33] A. Ballato, "Modeling piezoelectric and piezomagnetic devices and structures via equivalent networks," *IEEE Transactions on Ultrasonics, Ferroelectrics, and Frequency Control*, vol. 48, pp. 1189–1240, 9 2001.

[34] G. Hayward and M. Jackson, "Discrete-time modeling of the thickness mode piezoelectric transducer," *IEEE Transactions on Sonics and Ultrasonics*, vol. 31, pp. 137–150, 5 1984.

[35] ——, "A lattice model of the thickness-mode piezoelectric transducer," *IEEE Transactions on Ultrasonics, Ferroelectrics and Frequency Control*, vol. 33, pp. 41–50, 1 1986.

[36] S.-H. Wang and M.-C. Tsai, "Dynamic modeling of thickness-mode piezoelectric transducer using the block diagram approach," *Ultrasonics*, vol. 51, pp. 617–624, 7 2011.

[37] R. Giampiccolo, A. Bernardini, G. Gruosso, P. Maffezzoni, and A. Sarti, "Multidomain modeling of nonlinear electromagnetic circuits using wave digital filters," *International Journal of Circuit Theory and Applications*, vol. 50, pp. 539–561, 2022.

[38] A. Bernardini and A. Sarti, "Towards inverse virtual analog modeling," 9 2019.

[39] A. Bernardini, L. Bianchi, and A. Sarti, "Loudspeaker virtualization–part i: Digital modeling and implementation of the nonlinear transducer equivalent circuit," *Signal Processing*, vol. 202, p. 108720, 1 2022.

[40] ——, "Loudspeaker virtualization–part ii: The inverse transducer model and the direct-inverse-direct chain," *Signal Processing*, p. 108713, 8 2022.

[41] S. Morris and C. Hutchens, "Implementation of mason's model on circuit analysis programs," *IEEE Transactions on Ultrasonics, Ferroelectrics and Frequency Control*, vol. 33, pp. 295–298, 5 1986.

[42] H. Wang, Y. Ma, Q. Zheng, K. Cao, Y. Lu, and H. Xie, "Review of recent development of mems speakers," *Micromachines 2021, Vol. 12, Page 1257*, vol. 12, p. 1257, 10 2021.

[43] L. O. Chua, C. Desoer, and E. Kuh, *Linear and Nonlinear Circuits*. McGraw-Hill, 1987.

[44] A. Fettweis, "Reciprocity, inter-reciprocity, and transposition in wave digital filters," *International Journal of Circuit Theory and Applications*, vol. 1, pp. 323–337, 12 1973.

[45] A. Bernardini, K. J. Werner, J. O. Smith, and A. Sarti, "Generalized wave digital filter realizations of arbitrary reciprocal connection networks," *IEEE Transactions on Circuits and Systems I: Regular Papers*, vol. 66, pp. 694–707, 2019.

[46] G. O. Martens and H. H. Lê, "Wave digital adaptors for reciprocal second-order sections," *IEEE Transactions on Circuits and Systems*, vol. 25, pp. 1077–1083, 10 1978.

[47] S. Seshu and M. B. Reed, *Linear Graphs and Electrical Networks*. AddisonWesley Publishing Company, Inc. Reading, 1961.
[48] J. H. Huang, H. C. Her, Y. C. Shiah, and S. J. Shin, "Electroacoustic simulation and experiment on a miniature loudspeaker for cellular phones," *Journal of Applied Physics*, vol. 103, p. 033502, 2 2008. [Online]. Available: https://aip.scitation.org/doi/abs/10.1063/1.2837112
[49] M. Redwood, "Transient performance of a piezoelectric transducer," *Journal of the Acoustical Society of America*, vol. 33, pp. 527–536, 1961.
[50] S. A. Morris and C. G. Hutchens, "Implementation of mason's model on circuit analysis programs," *IEEE Transactions on Ultrasonics, Ferroelectrics, and Frequency Control*, vol. 33, pp. 295–298, 1986.
[51] C. R. Phillips and N. T. Nagle, *Digital control system analysis and design*. Englewood Cliffs, NJ: Prentice Hall, 1984.
[52] A. Bernardini, P. Maffezzoni, and A. Sarti, "Vector wave digital filters and their application to circuits with two-port elements," *IEEE Transactions on Circuits and Systems I: Regular Papers*, vol. 68, pp. 1269–1282, 2021.

Riccardo Giampiccolo (GSM'20) received both the B.S. and the M.S. degrees in electronics engineering from the Politecnico di Milano, Italy, in 2017 and 2020, respectively. He is currently a Ph.D. Candidate in information technology at the Dipartimento di Elettronica, Informazione e Bioingegneria of the Politecnico di Milano, Italy. His main research interests include audio signal processing, nonlinear systems, and signal processing methodologies for small-size transducers in consumer electronics.

Alberto Bernardini (S'16-M'19) received the B.S. degree from the University of Bologna, Italy, and M.S. degree (cum laude) from the Politecnico di Milano, Italy, both in computer engineering, in 2012 and 2015, respectively. In 2019, he received his Ph.D. degree (cum laude) in information engineering from Politecnico di Milano, Italy, where he is currently an Assistant Professor. His main research interests include audio signal processing, computational acoustics, and modeling of nonlinear systems. He authored more than 30 publications in international journals and proceedings of international conferences. He is also the first author of an international patent.

Augusto Sarti (M'04-SM'13) received his Ph.D. Information Engineering from the University of Padova, Italy, in 1993, with a joint graduate program with University of California, Berkeley. In 1993, he joined the Faculty of the Politecnico di Milano, Italy, where he is currently a Full Professor. In 2013, he also joined the University of California, Davis. He coordinates the activities of the Musical Acoustics Laboratory and the Sound and Music Computing Laboratory of the Politecnico di Milano. He promoted/coordinated and/or contributed to numerous European projects in the area of multimedia signal processing. He has coauthored over 300 scientific publications on international journals and congresses and numerous patents in the multimedia signal processing area. His main research interests are in the area of audio and acoustic signal processing, with particular focus on sound analysis, synthesis, and processing; space-time audio processing; geometrical acoustics; music information extraction and music modeling. He served in the IEEE Technical Committee on Audio and Acoustics Signal Processing for two terms. He served as Associate Editor of IEEE/ACM Tr. On Audio Speech and Language Processing, and as Senior Area Editor of IEEE Signal Processing Letters, and in 2017 he received the "Outstanding Editorial Board Member Award" by the IEEE Signal Processing Society. He co-chaired the IEEE Intl. Conf. on Advanced Video and Signal based Surveillance (AVSS-05); he chaired the Digital Audio Effects conference (DAFx-09); and he co-chaired the IEEE Intl. Workshop on Applications of Signal Processing to Audio and Acoustics (WASPAA-19). He was in the organizing committees of numerous International Conferences, including IEEE ICASSP-14; the ACM/IEEE Intl. Conf. on Distributed Smart Cameras (ICDSC-09); the IEEE Intl. Workshop on Haptic Audio-Visual Environment and Game (HAVE-09); and the European Signal Processing Conference (EUSIPCO-2018). He is currently serving in the EURASIP board of directors.